






Magnetotransport studies of Fe vacancy-ordered $\text{Fe}_{4+\delta}\text{Se}_5$ nanowires

Keng-Yu Yeh^{a,b,c,1}, Tung-Sheng Lo^{a,1} , Phillip M. Wu^{a,d,2}, Kuei-Shu Chang-Liao^c, Ming-Jye Wang^{a,e} , and Maw-Kuen Wu^{a,2} 

^aInstitute of Physics, Academia Sinica, 115 Taipei, Taiwan; ^bTaiwan International Graduate Student Program, Academia Sinica, 115 Taipei, Taiwan; ^cDepartment of Engineering and System Science, National Tsing Hua University, 300 Hsinchu, Taiwan; ^dBitSmart LLC, San Mateo, CA 94403; and ^eInstitute of Astronomy and Astrophysics, Academia Sinica, 115 Taipei, Taiwan

Contributed by Maw-Kuen Wu, April 6, 2020 (sent for review January 21, 2020; reviewed by C. L. Chien and M. Brian Maple)

We studied the electrical transport of $\text{Fe}_{4+\delta}\text{Se}_5$ single-crystal nanowires exhibiting $\sqrt{5} \times \sqrt{5}$ Fe-vacancy order and mixed valence of Fe. $\text{Fe}_{4+\delta}\text{Se}_5$ compound has been identified as the parent phase of FeSe superconductor. A first-order metal-insulator (MI) transition of transition temperature $T_{\text{MI}} \sim 28$ K is observed at zero magnetic fields (B). Colossal positive magnetoresistance emerges, resulting from the magnetic field-dependent MI transition. T_{MI} demonstrates anisotropic magnetic field dependence with the preferred orientation along the c axis. At temperature $T < \sim 17$ K, the state of near-magnetic field-independent resistance, which is due to spin polarized even at zero fields, preserves under magnetic fields up to $B = 9$ T. The Arrhenius law shift of the transition on the source-drain frequency dependence reveals that it is a nonoxide compound with the Verwey-like electronic correlation. The observation of the magnetic field-independent magnetoresistance at low temperature suggests it is in a charge-ordered state below $T \sim 17$ K. The results of the field orientation measurements indicate that the spin-orbital coupling is crucial in $\sqrt{5} \times \sqrt{5}$ Fe vacancy-ordered $\text{Fe}_{4+\delta}\text{Se}_5$ at low temperatures. Our findings provide valuable information to better understand the orbital nature and the interplay between the MI transition and superconductivity in FeSe-based materials.

Verwey transition | Fe-vacancy order | colossal magnetoresistance

The discovery of FeAs-based (1) and FeSe-based (2) superconductors created an exciting platform for better understanding the physics of high-temperature superconductivity. The observation of a wide range of superconducting transition temperatures, with the highest confirmed Cooper pair formation temperature up to 75 K in monolayer FeSe film (3), is indeed intriguing and provides a unique opportunity to gain more insight into the origin of high-temperature superconductivity.

The multiple-orbital nature of FeSe, combined with spin and charge degrees of freedom, results in the observation of many interesting phenomena such as nematicity (4, 5), orbital-selective Mott transition (6–8), and orbital ordering (9). There are suggestions that the orbital fluctuation may provide a new channel for realizing superconductivity (10, 11). Direct determination of the correlation between the orbital nature of the low-energy electronic states and the superconducting gap is crucial to understand the superconductivity mechanism of the Fe-based superconductors.

It has been a debate whether there exists an antiferromagnetic Mott insulating parent phase, similar to the cuprate superconductors, for FeSe superconductors. Chen et al. (12) reported the existence of the Fe_4Se_5 phase with $\sqrt{5} \times \sqrt{5}$ Fe-vacancy order and argued this Fe_4Se_5 phase to be the parent phase of FeSe superconductors. Theoretical simulation shows that the ground state of $\sqrt{5} \times \sqrt{5}$ Fe vacancy-ordered Fe_4Se_5 has a pair-checkerboard antiferromagnetic order, and the Fe $3d$ orbitals govern the low-energy physics (13). Analogously, recent studies demonstrated unambiguously that the $\text{K}_2\text{Fe}_4\text{Se}_5$, which exhibits a $\sqrt{5} \times \sqrt{5}$ Fe-vacancy order accompanied with an antiferromagnetic order (14, 15), is the parent phase of the superconductor $\text{K}_2\text{Fe}_{4+x}\text{Se}_5$ (16,

17). Detailed studies of the Fe vacancy in $\text{K}_2\text{Fe}_{4+x}\text{Se}_5$ reveal that its order/disorder is directly associated with superconductivity. It is worth noting that the Fe vacancy-ordered $\text{K}_2\text{Fe}_4\text{Se}_5$ exhibits an anomalous magnetic transition, similar to the Verwey transition observed in magnetite (Fe_3O_4), at around 125 K where the material shows Mott transition (16).

Fe vacancy-ordered Fe_4Se_5 is expected to exhibit mixed valence of Fe^{2+} and Fe^{3+} . A mixed-valence compound may show correlations among the orders of charge, spin, and orbital (18). In a former study, crystal-like Fe_4Se_5 sheets show a metal-insulator (MI) transition and a drop in magnetic susceptibility at low temperatures (12), reminiscent of the Verwey transition in the mixed-valence Fe_3O_4 (19). We have successfully synthesized FeSe mesoscale materials with various Fe-vacancy orders (12, 20, 21). The recent more detailed investigations on the properties of Fe-deficient $\text{Fe}_{4+\delta}\text{Se}_5$ unambiguously demonstrated two key issues: 1) the $\text{Fe}_{4+\delta}\text{Se}_5$ with Fe-vacancy order is a Mott insulator showing Verwey-like transition; 2) $\text{Fe}_{4+\delta}\text{Se}_5$ is the parent compound of the FeSe superconductors (12, 20).

In this work, we present the electrical transport of the Fe-deficient $\text{Fe}_{4+\delta}\text{Se}_5$ single-crystal nanowires with $\sqrt{5} \times \sqrt{5}$ -ordered Fe vacancies and mixed valence of Fe. There are two main reasons to use nanowire in this study. First, the nanowire is high-quality single crystal with long length for transport measurements. Second, it has been shown in single-crystal Fe_3O_4 nanowire an Arrhenius frequency dependence of the resistive

Significance

This work reveals that $\text{Fe}_{4+\delta}\text{Se}_5$ with ordered Fe vacancy is a nonoxide compound with the Verwey-like electronic correlation. Detailed measurements showing magnetic field-independent magnetoresistance at low temperature suggest it is in a charge-ordered state below $T \approx 17$ K. The results of the field orientation measurements indicate that the spin-orbital coupling is crucial in $\sqrt{5} \times \sqrt{5}$ Fe vacancy-ordered $\text{Fe}_{4+\delta}\text{Se}_5$ at low temperatures. Our findings provide valuable information to better understand the orbital nature and the interplay between the metal-insulator transition and superconductivity in FeSe-based materials.

Author contributions: P.M.W., M.-J.W., and M.-K.W. designed research; K.-Y.Y., T.-S.L., and P.M.W. performed research; K.-S.C.-L. and M.-J.W. contributed new reagents/analytic tools; K.-Y.Y., T.-S.L., P.M.W., K.-S.C.-L., M.-J.W., and M.-K.W. analyzed data; and K.-Y.Y., T.-S.L., P.M.W., and M.-K.W. wrote the paper.

Reviewers: C.L.C., Johns Hopkins University; and M.B.M., University of California San Diego.

The authors declare no competing interest.

This open access article is distributed under [Creative Commons Attribution-NonCommercial-NoDerivatives License 4.0 \(CC BY-NC-ND\)](https://creativecommons.org/licenses/by-nc-nd/4.0/).

¹K.-Y.Y. and T.-S.L. contributed equally to this work.

²To whom correspondence may be addressed. Email: mkwu@phys.sinica.edu.tw or pmwu@gate.sinica.edu.tw.

This article contains supporting information online at <https://www.pnas.org/lookup/suppl/doi:10.1073/pnas.2000833117/-DCSupplemental>.

First published May 22, 2020.

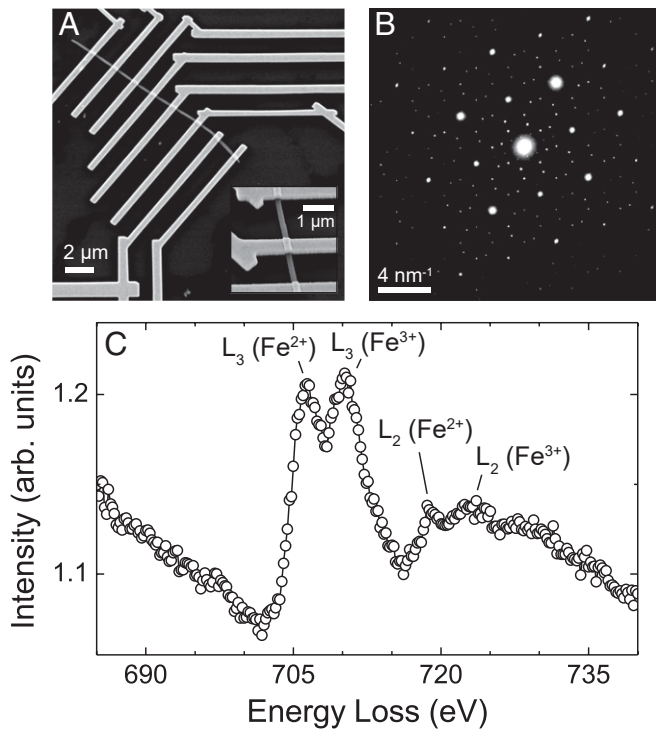


Fig. 1. Sample characterization. (A) The SEM image of an $\text{Fe}_{4+6}\text{Se}_5$ nanowire after deposited electrical leads. A, *Inset* is the tilted SEM image, showing that the nanowire has width of ~ 180 nm and thickness of ~ 60 nm. (B) The SAED pattern of a $\beta\text{-Fe}_{4+6}\text{Se}_5$ nanowire along the c -axis direction. (C) The EELS spectrum of Fe $L_{2,3}$ edges of an $\text{Fe}_{4+6}\text{Se}_5$ nanowire, showing the mixed valence of Fe.

transition, which was associated with the relaxation of charge order after the ordering state was excited by a direct-current voltage. We first observe a first-order MI transition with an onset transition temperature at $T \sim 28$ K at zero magnetic fields. We use the magnetotransport to better understand the spin-relevant correlation with the phase transition and employ alternative-current (AC) excitation to investigate the underlying nature of the transition. Our data show, similar to that observed in Fe_3O_4 nanowire, a strong frequency dependence of the MI resistive transition, and the spin-orbital coupling is crucial for the transition observed. The observation of weak magnetic field in the nanowires below 17 K provides additional evidence that the low-temperature state is an antiferromagnetic charge order state.

The $\text{Fe}_{4+6}\text{Se}_5$ nanowires were grown by the on-film formation method (21). The nanowires are typically rectangular strips with a few hundred-nanometer width and several tens of micrometers in length as shown by the scanning electron microscope (SEM) image in Fig. 1A. We used the 30-nm-thick Si_3N_4 membranes to hold the nanowires for the benefit of characterizing the nanowires in situ by the transmission electron microscope (TEM). The electrical leads, patterned by electron beam lithography with 90 °C baked PMMA (polymethyl methacrylate), were made of Au/Ti bilayer (150/30 nm) after the surface oxide layer of the nanowires was removed by Ar plasma. The resistances of the nanowires were measured by the four-probe method and lock-in technique with an AC excitation less than 300 nA. Sample temperature and external magnetic field are controlled by physical property measurement system, and the field orientation to the sample is changed by rotating the sample via a rotation insert.

For sample characterizations, we used TEM to obtain the selected area electron diffraction (SAED) pattern, the scanning TEM–energy-dispersive X-ray spectrometer (EDS) for element

analysis, and the electron energy loss spectroscopy (EELS) to determine the Fe valence. The element mappings show uniform distributions of Fe and Se on the nanowire (*SI Appendix, Fig. S1*). The ratio between Fe and Se in this nanowire is 4.48/5 according to EDS analysis. As shown in Fig. 1B, the SAED pattern reveals that the $\text{Fe}_{4+6}\text{Se}_5$ nanowire is a single crystal with a tetragonal structure, where the b axis is parallel to the longitudinal axis of the nanowire, the c axis is perpendicular, and the a axis is parallel to the wide side of the nanowire. The electron diffraction also clearly shows the superstructure related to the $\sqrt{5} \times \sqrt{5}$ Fe-vacancy order (12). The a -axis lattice constant is estimated to be 3.73 Å. The EELS data in Fig. 1C demonstrate the absorption peaks for the Fe L_3 edge (Fe^{2+} at 706.4 eV and Fe^{3+} at 710.2 eV) and the Fe L_2 edge (Fe^{2+} at 718.4 eV and Fe^{3+} at 723.5 eV), confirming the existence of mixed-valence state of Fe^{2+} and Fe^{3+} . The estimated ratio of $\text{Fe}^{2+}/\text{Fe}^{3+}$ is close to 1/1 from the spectrum (*SI Appendix, Fig. S2*).

We first measured the temperature (T) dependence of the resistance (R) with the temperature control rate of 1 K/min and the AC excitation frequency at 37 Hz. Fig. 2 shows the R vs. T in cooling and warming measured at different magnetic fields B parallel to the c axis. The data show clearly the thermal hysteresis of the transition. At $B = 0$, R undergoes an MI transition with the transition-onset temperature $T_{\text{MI}} \sim 28$ K, where T_{MI} is defined as the temperature at which the thermal hysteresis appears. As temperature decreases, R drastically increases from about 15 k Ω ; reaches a resistance peak of 0.74 M Ω at 21.0 K; then decreases to about 0.4 M Ω at T_o , which is defined as the temperature where the thermal hysteresis disappears; and finally accesses a plateau regime. The thermal hysteresis of $R(T)$ indicates the transition is first order, further confirmed by the applied magnetic field B , which enhances the thermal hysteresis loop. The transition, including the aforementioned resistance peak, shifts toward a higher-temperature regime at a higher magnetic field, making both T_{MI} and T_o increase with increasing B , as shown in Fig. 2, *Lower Inset*, which displays the phase diagram of the transition. At $T > \sim 30$ K, the resistance enhances as magnetic fields increase. The resistance peak value does not change monotonically with magnetic fields. Fig. 2, *Upper Inset* shows more details of the $R(T)$ at $T < 24$ K. A dip is found at $T \sim 19$ K at $B = 0$ T and shifts to higher temperature with increasing

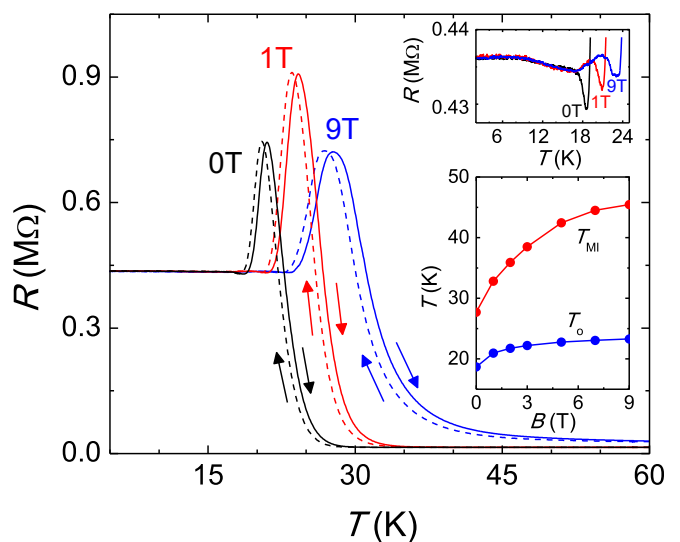


Fig. 2. Magnetic field dependence of $R(T)$ with the field direction along the c axis, including results measured in warming and cooling. *Upper Inset* shows $R(T)$ in warming at $T < 25$ K. *Lower Inset* shows the phase diagram on the T - B plot, including T_{MI} and T_o derived from $R(T)$ at different magnetic fields.

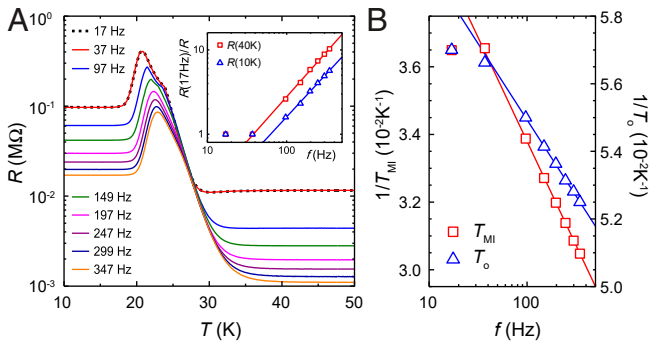


Fig. 3. The AC excitation frequency (f) dependence on the transition. (A) $R(T)$ curves measured in warming at different f . The curves of 17 and 37 Hz are almost overlapped. A, *Inset* shows the f dependence of conductance $1/R(10\text{ K})$ and $1/R(40\text{ K})$, normalized by the values at $f = 17\text{ Hz}$. The solid lines show $1/R \propto f^\alpha$, where α is 1.06 for $1/R(40\text{ K})$ and 1.02 for $1/R(10\text{ K})$. (B) $1/T_a$ vs. f , where T_a is T_{MI} or T_o . The solid lines depict $1/T_a = (-k_B/E_a)\ln(f) + \text{constant}$, an alternative expression of the Arrhenius law. E_a is 32.3 meV for T_{MI} and 44.0 meV for T_o .

B. The $R(T)$ plateau at $T < 17\text{ K}$ is closely B independent up to $B = 9\text{ T}$ and reaches $R = 0.436\text{ M}\Omega$ at $T < 8\text{ K}$.

To gain further insight into the MI transition of the $\text{Fe}_{4+\delta}\text{Se}_5$ nanowire, we investigated the AC source-drain frequency (f) dependence of $R(T)$ at $B = 0\text{ T}$. The f -dependent experiment was carried out on another section of the same nanowire. Fig. 3A shows that R decreases with increasing frequency while nearly fixed at $T \sim 28\text{ K}$ [$\sim T_{\text{MI}}(0\text{T})$], suggesting that $T_{\text{MI}}(0\text{T})$ is the critical point of the phase transition. (We have carefully checked to rule out the possibility of the capacitive coupling of the sample with the Si_3N_4 substrate that leads to the observed frequency dependence of R [SI Appendix, Fig. S3].) The results are similar to that reported by Gooth et al. (22) on the f dependence of the Verwey transition in single-crystal Fe_3O_4 nanowires. The kinks occurring in the transition regime may result from the discrete jumps in order parameters, which were observed in the MI transitions of mesoscale strongly correlated systems (23–25). As shown in Fig. 3A, *Inset*, $1/R \propto f^\alpha$ with $\alpha \sim 1$ for $T < T_o$ and $T > T_{\text{MI}}$ as $f > 37\text{ Hz}$. The linear f dependence of $1/R$ was also found in Fe_3O_4 nanowires and was ascribed to the correlated hopping. As shown in Fig. 3B, the change in T_{MI} and T_o at higher frequency ($f > 37\text{ Hz}$) follows the Arrhenius law $f \propto \exp(-E_a/k_B T_a)$, where T_a is T_{MI} or T_o and E_a is the activation energy. The Arrhenius law f dependence was also reported in the Fe_3O_4 nanowire study. E_a values are 32.3 and 44.0 meV for T_{MI} and T_o , respectively. The increase of E_a is $\Delta E_a \sim 11.7\text{ meV}$ by cooling through the transition.

When an Fe_3O_4 single crystal was cooled through the Verwey transition of the transition temperature $T_V \sim 125\text{ K}$, the energy-gap change of $\Delta E \sim 50\text{ meV}$ was found and attributed to the emergence of long-range charge order (26), which is related to the formation of orbital order (27) and the associated structure change (28). For the $\text{Fe}_{4+\delta}\text{Se}_5$ nanowire, the $T_{\text{MI}}/\Delta E_a \sim 30\text{ K}/11.7\text{ meV} = 2.56\text{ K/meV}$ is comparable with the value of $T_V/\Delta E \sim 125\text{ K}/50\text{ meV} = 2.5\text{ K/meV}$ for the single-crystal Fe_3O_4 (26–28). Therefore, the E_a enhancement observed in the $\text{Fe}_{4+\delta}\text{Se}_5$ nanowire could be attributed to the Verwey-like energy-gap expansion. These results strongly support that the $\text{Fe}_{4+\delta}\text{Se}_5$ is a nonoxide compound exhibiting Verwey-like MI transition.

The $\text{Fe}_{4+\delta}\text{Se}_5$ nanowire provides us an opportunity to investigate the underline physics of the Verwey-like transition in depth. Subsequently, we measured the magnetic field effects on the resistive behavior near the transition. The results are shown in Fig. 4, which shows the magnetoresistance $R(B)$ of the

nanowire at different temperatures with the magnetic fields parallel to the c axis. Fig. 4A displays $\Delta R(B)/R(0\text{T})$ and $R(B)$ at $23\text{ K} \leq T \leq 35\text{ K}$, where $\Delta R(B) = R(B) - R(0\text{T})$, and Fig. 4B shows $R(B)$ at $T \leq 22\text{ K}$. Colossal positive magnetoresistance with $\Delta R(B)/R(0\text{T}) > 10$ is observed at temperature range $25\text{ K} < T < 35\text{ K}$, which is within the transition window. An $R(B)$ peak emerges at $20\text{ K} \leq T \leq 26\text{ K}$ and with decreasing T , shifts to lower magnetic fields. The magnetic field dependences of the temperatures at which $R(B)$ and $R(T)$ show peaks follow the same curve, as shown in Fig. 4B, *Inset*. $R(B)$ at $T \leq 17\text{ K}$ is negligibly B dependent [i.e., $R(B) \sim R(0\text{T})$]. It is noted that $R(B)$ also becomes nearly constant when the magnetic fields are sufficiently high at $17\text{ K} < T < 23\text{ K}$, and the B range of the near-constant $R(B)$ is extended toward low fields by lowering T . This suggests that the nearly B -independent state at $T \leq 17\text{ K}$ is spin polarized.

It has been demonstrated that the resistivity at the (antiferromagnetic) charge-ordered state of the perovskite-type manganese oxides $\text{Pr}_{0.5}\text{Sr}_{0.5}\text{MnO}_3$ (29) and $\text{Pr}_{0.5}\text{Ca}_{0.5}\text{MnO}_3$ (30) is weakly magnetic field dependent below the MI transition. Therefore, the almost magnetic field independent of the resistance in our nanowires below 17 K, which is $\sim 10^9$ lower than the MI transition, is the manifest of the charge order. This observation provides additional evidence to show that the MI transition in $\text{Fe}_{4+\delta}\text{Se}_5$, similar to the Fe_3O_4 system, is related to the well-known Verwey transition,

The $\Delta R(B)/R(0\text{T})$ at $T \geq 22\text{ K}$ can be well described by the relation $\Delta R(B)/R(0\text{T}) = A/[1 + (B/B_0)^{-r}]$ for $B < B_0$, where A and B_0 are the fitting parameters, as shown in Fig. 4C. An analogous formula with $r = 2$ was derived theoretically for the magnetoresistance of graphite with the magnetic field direction along the c axis and perpendicular to the current direction (31).

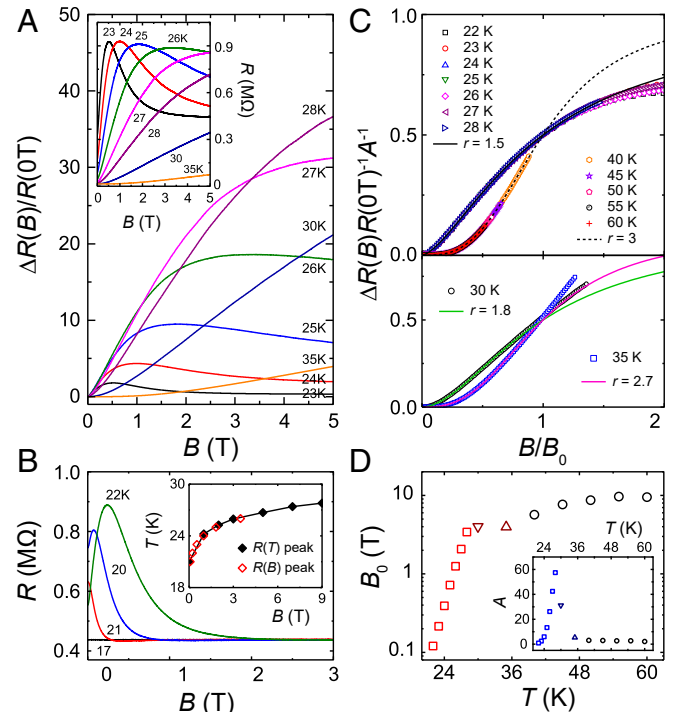


Fig. 4. Magnetoresistance with the direction of magnetic fields parallel to the c axis at different temperatures. Temperature is changed in steps by warming. (A) $\Delta R(B)/R(0\text{T})$ at $23\text{ K} \leq T \leq 35\text{ K}$, with the respective $R(B)$ shown in *Inset*. (B) $R(B)$ at $T \leq 22\text{ K}$. B, *Inset* shows the positions of the maximum of $R(B)$ and $R(T)$ peaks. (C) $\Delta R(B)R^{-1}(0\text{T})A^{-1}$ vs. B/B_0 and the scaling curves $\Delta R(B)R^{-1}(0\text{T})A^{-1} = 1/[1 + (B/B_0)^{-r}]$ of $r = 3, 2.7, 1.8$, and 1.5. (D) B_0 plotted vs. T with different symbols representing different r exponents. D, *Inset* shows A vs. T .

At $B \ll B_0$, $A/[1 + (B/B_0)^r] \sim A(B/B_0)^{-r}$ gives a power law relation. The data fit well for fields below B_0 (i.e., $B/B_0 < 1$) but with different exponents at different temperature ranges. At temperature range $60 \text{ K} \geq T \geq 40 \text{ K}$, the exponent $r = 3$; at $28 \text{ K} \geq T \geq 22 \text{ K}$, $r = 1.5$. At $40 \text{ K} > T > 28 \text{ K}$, r varies between 1.5 and 3. The A and B_0 values obtained are summarized in Fig. 4D. B_0 decreases with lowering temperature and has a clear transition around $T_{\text{MI}}(0\text{T})$ ($\sim 28 \text{ K}$). The large enhancement of A around $T_{\text{MI}}(0\text{T})$ is related to the emergence of the colossal positive magnetoresistance. As magnetoresistance depends on the topology of the Fermi surface (32), the distinct difference in magnetoresistance may suggest the change of the Fermi surface topology over the first-order transition.

We further investigated the magnetic field orientation dependence of the transition by rotating the nanowire an angle ϕ_a (ϕ_b) with the rotation axis along the a axis (b axis) so that the field is parallel to c axis at ϕ_a (ϕ_b) = 0. The ϕ_a - and ϕ_b -dependent experiments were carried out on two sections of the same nanowire. Fig. 5 A and B shows the $R(T)$ results in magnetic fields at different ϕ_a and ϕ_b , respectively. At $B = 9 \text{ T}$, the first-order transition shifts toward lower temperature as the magnetic field direction changes from parallel to perpendicular to the c axis. At $T \leq 17 \text{ K}$, regardless of the orientation and magnitude of the fields, the resistance is only weakly magnetic field dependent. On the other hand, the magnetic field orientation dependence of the R peak value is complex.

Fig. 5 A, *Inset* and B, *Inset* show $\Delta R(B)/R(0\text{T})$ plotted vs. the magnetic field components parallel to the c axis, $B \cdot |\cos(\phi_a)|$ and $B \cdot |\cos(\phi_b)|$, respectively, illustrating the magnetic field orientation dependence of $\Delta R(B)/R(0\text{T})$ at $T \geq 40 \text{ K}$. In Fig. 5 B, *Inset*, $\Delta R(B)/R(0\text{T})$ values at different ϕ_b values can be scaled on a single curve and indicate that $\Delta R(B, \phi_b)/R(0\text{T}) = A/[1 + (B \cdot |\cos(\phi_b)|/B_0)^{-3}]$. The scaling manifests a two-dimensional (2D) electrical transport characteristic (33, 34) and suggests that the

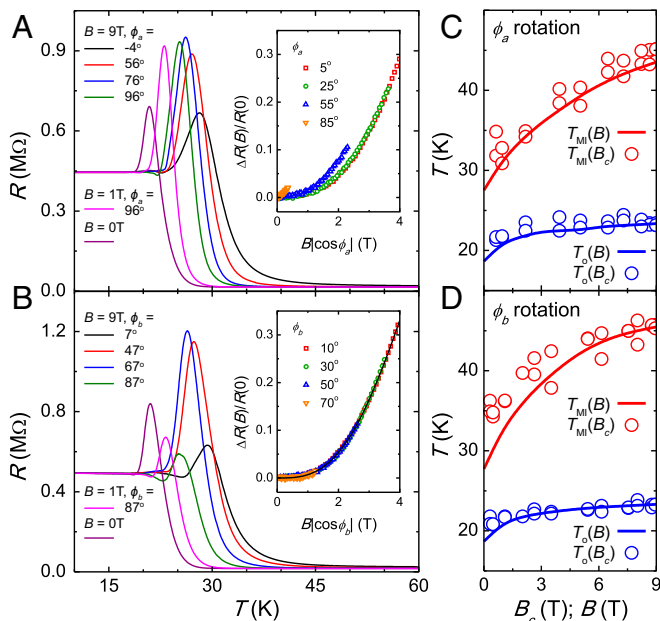


Fig. 5. Magnetic field orientation dependence. (A and B) $R(T)$ measured in warming at magnetic fields of different ϕ_a and ϕ_b , respectively. A, *Inset* and B, *Inset* show $\Delta R(B)/R(0\text{T})$ vs. $B \cdot |\cos(\phi_a)|$ and $B \cdot |\cos(\phi_b)|$, respectively, at $T = 40 \text{ K}$. The solid line in B, *Inset* is the curve of $\Delta R(B)/R(0\text{T}) = A/[1 + (B \cdot |\cos(\phi_b)|/B_0)^{-3}]$ with $A = 1.26$, $\phi_b = 0^\circ$, and $B_0 = 5.65 \text{ T}$. (C and D) T_{MI} (red circles) and T_o (blue circles) vs. B_c , the magnetic field component along the c axis at $B = 9 \text{ T}$, in ϕ_a and ϕ_b rotations. The solid lines are T_{MI} and T_o vs. B as the magnetic fields parallel to the c axis.

electrical transport in Fe_4Se_5 is on the ab plane. Nevertheless, in ϕ_a rotation, as shown in Fig. 5 A, *Inset*, $\Delta R(B)/R(0\text{T})$ cannot be scaled on a single curve and suggests that small magnetoresistive contribution is induced by the magnetic field components parallel to the current direction, which could be attributed to the spin-orbital interaction (35).

Fig. 5 C and D displays the $T_{\text{MI}}(T_o)$ vs. B_c , the magnetic field components parallel to the c axis at $B = 9 \text{ T}$ for different ϕ_a and ϕ_b [i.e., $B_c = 9\text{T} \times |\cos(\phi_a)|$ and $B_c = 9\text{T} \times |\cos(\phi_b)|$, respectively] for $-180^\circ \leq \phi_a, \phi_b < 180^\circ$. The $T_{\text{MI}}(T_o)$ values at B_c scatter along the trace of $T_{\text{MI}}(T_o)$ vs. B at $\phi_a = \phi_b = 0^\circ$, where the magnetic fields are parallel to the c axis. The field-induced enhancements of T_{MI} and T_o are dominated by magnetic field components along the c axis. As the $T_o(B)$ traces of $\phi_a = \phi_b = 0^\circ$ are close to the nearly B -independent state of spin polarization, the B_c -dependent T_o indicates that the c axis is the preferred direction to polarize. The interactions between spin, orbital, and lattice should be taken into account to realize the c axis-preferred field dependence on the transition and the spin polarization. The rigidity of resistance under magnetic fields at $T < \sim 17 \text{ K}$ suggests a spin-polarized one-dimensional (1D) conduction (36).

For Fe_4Se_5 with the $\sqrt{5} \times \sqrt{5}$ Fe-vacancy order, the low-energy physics is dominated by Fe $3d$ orbitals (13). It is noted that in the $\sqrt{5} \times \sqrt{5}$ Fe vacancy-ordered $\text{K}_2\text{Fe}_4\text{Se}_5$ compound, the Fe ions show large saturated magnetic moments at low temperature, and the Fe magnetic moments form antiferromagnetic order with the c axis as the magnetic easy axis (14). Accordingly, we attribute the c axis-preferred magnetic field dependence to the spin-orbital coupling in tetragonal $\text{Fe}_{4+\delta}\text{Se}_5$, in which Fe $3d$ orbitals also play a major role. Thus, the spin-orbital coupling is essential for the near-magnetic field-independent state and spin polarization at $T < \sim 17 \text{ K}$ as well. The 1D characteristic of our sample might make the charge order state even more robust to magnetic field.

The observed $R(T)$ peak emerging in the transition regime may be associated with the cross-over from the 2D to 1D-like transport on cooling. It is noted that a peak-like feature has been observed in 3D topological insulators and is attributed to the existence of metallic topological surface states (37–40). In addition, an interesting recent development regarding the FeSe and related compounds is the potential realization of topological superconductivity in these materials (41). It was argued that the presence of topological phases is highly dependent on the bond length between the apical height of the Se to Fe atoms. Therefore, it certainly will be valuable to investigate in more detail whether there exists the topological feature in the Fe vacancy-ordered Fe_4Se_5 .

In summary, we studied the electrical transport of tetragonal $\text{Fe}_{4+\delta}\text{Se}_5$ nanowires exhibiting $\sqrt{5} \times \sqrt{5}$ Fe-vacancy order and mixed-valence state of Fe^{2+} and Fe^{3+} . A first-order MI transition with $T_{\text{MI}} \sim 28 \text{ K}$ is observed at zero magnetic fields. The activation energy from the Arrhenius law f dependence of the transition suggesting the transition is related to the Verwey-like electronic correlation. Thus, a Verwey-like transition is observed in a nonoxide compound. The results of the magnetic field-dependent T_{MI} and T_o indicate the c axis is the magnetic preferred orientation. The field effect on T_{MI} and T_o also results in the observation of colossal positive magnetoresistance in the transition regime at temperature $25 \text{ K} < T < 35 \text{ K}$. Based on the results of the magnetoresistive and field orientation-dependent measurements, the observation of nearly magnetic field-independent $R(B)$ below $T \sim 17 \text{ K}$ is due to the spin polarization, which spontaneously occurs even without magnetic field. Furthermore, the near-magnetic field independence, as well as the c axis-preferred magnetic field dependence, can be attributed to the spin-orbital coupling in the tetragonal Fe vacancy-ordered $\text{Fe}_{4+\delta}\text{Se}_5$ nanowire.

It has been proposed, and later experimentally confirmed, that the multiple-orbital band structures of $3d$ orbitals of Fe make Fe-based superconductors to exhibit topological phases as band inversion and spin-orbital coupling are introduced (41). Our findings indicate that $\sqrt{5} \times \sqrt{5}$ Fe vacancy-ordered Fe_4Se_5 , having multiple-orbital nature (13), exhibits behavior correlated to strong spin-orbital coupling, which potentially can make topological phase transition happen. The results could provide critical information for better understanding the origin of superconductivity in FeSe-based superconductors and the orbital-related physics in the FeSe-based materials.

Materials and Methods

Nanowires. FeSe nanowires were grown by the on-film formation method (21). FeSe thin films on (100) MgO substrate were first deposited by the pulse-laser deposition and then annealed at 400 °C for 120 h under 5×10^{-7} torr for the nanowire growth. The nanowires prefer to grow near the edge of the film and can be easily detached and transferred to the surface of 30-nm-thick Si_3N_4 membrane on the $1 \times 1\text{-cm}$ Si_3N_4 substrate for further

lithography preparation and for in situ TEM observation as mentioned in the text.

Structure Characterization. A homemade TEM sample holder, which is fitted to the $1 \times 1\text{-cm}$ Si_3N_4 substrate with the Si_3N_4 membrane, was prepared for the single FeSe nanowire analysis. The FeSe nanowire samples were observed by the JEOL 2100F microscope equipped with an OXFORD X-Max EDX analyzer and Gatan GIF 863 Tridiem Electron Energy Loss Spectroscopy. The lattice constants were derived from interplanar spacings in the SAED patterns and analyzed by a nonlinear least squares cell refinement program.

Data Availability. We have provided all relevant data in the text and *SI Appendix*.

ACKNOWLEDGMENTS. We thank Dr. Chung-Chieh Chang for providing the nanowire samples and Dr. Peramaiyan Ganesan and Dr. Yen-Fu Liu (Institute of Physics, Academia Sinica) for valuable discussions. The work is supported by Ministry of Science and Technology Grant MOST108-2633-M-001-001 and Academia Sinica Thematic Research Grant AS-TP-106-M01.

1. Y. Kamihara, T. Watanabe, M. Hirano, H. Hosono, Iron-based layered superconductor $\text{La}[\text{O}_{1-x}\text{F}_x]\text{FeAs}$ ($x = 0.05\text{--}0.12$) with $T_c = 26$ K. *J. Am. Chem. Soc.* **130**, 3296–3297 (2008).
2. F.-C. Hsu et al., Superconductivity in the PbO-type structure $\alpha\text{-FeSe}$. *Proc. Natl. Acad. Sci. U.S.A.* **105**, 14262–14264 (2008).
3. R. Peng et al., Tuning the band structure and superconductivity in single-layer FeSe by interface engineering. *Nat. Commun.* **5**, 5044 (2014).
4. S. Avci et al., Magnetically driven suppression of nematic order in an iron-based superconductor. *Nat. Commun.* **5**, 3845 (2014).
5. R. Yu, J.-X. Zhu, Q. Si, Orbital selectivity enhanced by nematic order in FeSe. *Phys. Rev. Lett.* **121**, 227003 (2018).
6. M. Yi et al., Observation of temperature-induced crossover to an orbital-selective Mott phase in $\text{A}_x\text{Fe}_{2-y}\text{Se}_2$ ($\text{A}=\text{K}, \text{Rb}$) superconductors. *Phys. Rev. Lett.* **110**, 67003 (2013).
7. R. Yu, Q. Si, Orbital-selective Mott phase in multiorbital models for alkaline iron selenides $\text{K}_{1-x}\text{Fe}_{2-y}\text{Se}_2$. *Phys. Rev. Lett.* **110**, 146402 (2013).
8. J. Herbrich et al., Spin dynamics of the block orbital-selective Mott phase. *Nat. Commun.* **9**, 3736 (2018).
9. M. Yi, Y. Zhang, Z.-X. Shen, D. Lu, Role of the orbital degree of freedom in iron-based superconductors. *Npj Quantum Materials* **2**, 57 (2017).
10. T. Saito, S. Onari, H. Kontani, Orbital fluctuation theory in iron pnictides: Effects of As-Fe-As bond angle, isotope substitution, and Z_2 -orbital pocket on superconductivity. *Phys. Rev. B* **82**, 144510 (2010).
11. H. Kontani, S. Onari, Orbital-fluctuation-mediated superconductivity in iron pnictides: Analysis of the five-orbital hubbard-holstein model. *Phys. Rev. Lett.* **104**, 157001 (2010).
12. T.-K. Chen et al., Fe-vacancy order and superconductivity in tetragonal $\beta\text{-Fe}_{1-x}\text{Se}$. *Proc. Natl. Acad. Sci. U.S.A.* **111**, 63–68 (2014).
13. M. Gao, Q.-Z. Li, X.-W. Yan, J. Wang, Prediction of phonon-mediated superconductivity in borophene. *Phys. Rev. B* **95**, 024505 (2017).
14. W. Bao et al., A novel large moment antiferromagnetic order in $\text{K}_{0.8}\text{Fe}_{1.6}\text{Se}_2$ superconductor. *Chin. Phys. Lett.* **28**, 086104 (2011).
15. J. Zhao, H. Cao, E. Bourret-Courchesne, D.-H. Lee, R. J. Birgeneau, Neutron-diffraction measurements of an antiferromagnetic semiconducting phase in the vicinity of the high-temperature superconducting state of $\text{K}_x\text{Fe}_{2-y}\text{Se}_2$. *Phys. Rev. Lett.* **109**, 267003 (2012).
16. C.-H. Wang et al., Disordered Fe vacancies and superconductivity in potassium-intercalated iron selenide ($\text{K}_{2-x}\text{Fe}_{4+y}\text{Se}_5$). *Europhys. Lett.* **111**, 27004 (2015).
17. C.-H. Wang et al., Role of the extra Fe in $\text{K}_{2-x}\text{Fe}_{4+y}\text{Se}_5$ superconductors. *Proc. Natl. Acad. Sci. U.S.A.* **116**, 1104–1109 (2019).
18. C. M. Varma, Mixed-valence compounds. *Rev. Mod. Phys.* **48**, 219 (1976).
19. F. Walz, The Verwey transition—a topical review. *J. Phys. Condens. Matter* **14**, R285 (2002).
20. C.-C. Chang et al., Superconductivity in PbO-type tetragonal FeSe nanoparticles. *Solid State Commun.* **152**, 649 (2012).
21. H. Chang et al., Growth and characterization of superconducting $\beta\text{-FeSe}$ type iron chalcogenide nanowires. *Supercond. Sci. Technol.* **27**, 025015 (2014).
22. J. Gooth et al., Kinetics of the charge ordering in magnetite below the Verwey temperature. *J. Phys. Condens. Matter* **26**, 472202 (2014).
23. H.-Y. Zhai et al., Giant discrete steps in metal-insulator transition in perovskite manganite wires. *Phys. Rev. Lett.* **97**, 167201 (2006).
24. A. Sharoni, J. G. Ramirez, I. K. Schuller, Multiple avalanches across the metal-insulator transition of vanadium oxide nanoscaled junctions. *Phys. Rev. Lett.* **101**, 026404 (2008).
25. V. Uhlir, J. A. Arregi, E. E. Fullerton, Colossal magnetic phase transition asymmetry in mesoscale FeRh stripes. *Nat. Commun.* **7**, 13113 (2016).
26. J.-H. Park, L. H. Tjeng, J. W. Allen, P. Metcalf, C. T. Chen, Single-particle gap above the Verwey transition in Fe_3O_4 . *Phys. Rev. B* **55**, 12813 (1997).
27. D. Schrupp et al., High-energy photoemission on Fe_3O_4 : Small polaron physics and the Verwey transition. *Europhys. Lett.* **70**, 789 (2005).
28. A. Pimenov et al., Terahertz conductivity at the Verwey transition in magnetite. *Phys. Rev. B* **72**, 035131 (2005).
29. Y. Tomioka, A. Asamitsu, Y. Morimoto, H. Kuwahara, Y. Tokura, Collapse of a charge-ordered state under a magnetic field in $\text{Pr}_{1/2}\text{Sr}_{1/2}\text{MnO}_3$. *Phys. Rev. Lett.* **74**, 5108–5111 (1995).
30. Y. Tomioka, A. Asamitsu, H. Kuwahara, Y. Morimoto, Y. Tokura, Magnetic-field-induced metal-insulator phenomena in $\text{Pr}_{1-x}\text{Ca}_x\text{MnO}_3$ with controlled charge-ordering instability. *Phys. Rev. B Condens. Matter* **53**, R1689–R1692 (1996).
31. K. Noto, T. Tszuzuku, A simple two-band of galvanomagnetic effects in graphite in relation to the magnetic field azimuth. *Jpn. J. Appl. Phys.* **14**, 46 (1975).
32. S. Zhang, Q. Wu, Y. Liu, O. V. Yazyev, Magnetoresistance from Fermi surface topology. *Phys. Rev. B* **99**, 35142 (2019).
33. N. Kang et al., Two-dimensional quantum transport in free-standing InSb nanosheets. *Nano Lett.* **19**, 561–569 (2019).
34. Y. Sun, T. Yamada, S. Pyon, T. Tamegai, Structural-transition-induced quasi-two-dimensional Fermi surface in FeSe. *Phys. Rev. B* **94**, 134505 (2016).
35. S. Kokado, M. Tsunoda, K. Harigaya, A. Sakuma, Anisotropic magnetoresistance effects in Fe, Co, Ni, Fe_4N , and half-metallic ferromagnet: A systematic analysis. *J. Phys. Soc. Jpn.* **81**, 024705 (2012).
36. T.-M. Chen, A. C. Graham, M. Pepper, I. Farrer, D. A. Ritchie, Bias-controlled spin polarization in quantum wires. *Appl. Phys. Lett.* **93**, 32102 (2008).
37. S. Cai et al., Independence of topological surface state and bulk conductance in three-dimensional topological insulators. *Npj Quantum Materials* **3**, 62 (2018).
38. S. Wolgast et al., Low-temperature surface conduction in the Kondo insulator SmB_6 . *Phys. Rev. B* **88**, 180405 (2013).
39. Y. Luo, H. Chen, J. Dai, Z. Xu, J. D. Thompson, Heavy surface state in a possible topological Kondo insulator: Magnetothermoelectric transport on the (011) plane of SmB_6 . *Phys. Rev. B* **91**, 075130 (2015).
40. A. Dankert et al., Origin and evolution of surface spin current in topological insulators. *Phys. Rev. B* **97**, 125414 (2018).
41. N. Hao, J. Hu, Topological quantum states of matter in iron-based superconductors: From concept to material realization. *Natl. Sci. Rev.* **6**, 213–226 (2018).